Journal of Advanced Ceramics
2022, **11**(9): 1383–1390
https://doi.org/10.1007/s40145-022-0617-z
ISSN 2226-4108
CN 10-1154/TQ

Research Article

Fine-grained phosphors for red-emitting mini-LEDs with high efficiency and super-luminance

Yu KANG[a], Shuxing LI[b,*], Rundong TIAN[b], Guangzhu LIU[a,*], Haorui DONG[b], Tianliang ZHOU[b], Rong-Jun XIE[b,c,*]

[a]*College of Materials Science and Engineering*, *Liaoning Technical University*, *Fuxin 123000*, *China*
[b]*Fujian Provincial Key Laboratory of Surface and Interface Engineering for High Performance Materials*, *College of Materials*, *Xiamen University*, *Xiamen 361005*, *China*
[c]*State Key Laboratory of Physical Chemistry of Solid Surfaces*, *Xiamen University*, *Xiamen 361005*, *China*

Received: April 6, 2022; Revised: May 18, 2022; Accepted: May 25, 2022

Abstract: Mini-LED backlights, combining color conversion materials with blue mini-LED chips, promise traditional liquid crystal displays (LCDs) with higher luminance, better contrast, and a wider color gamut. However, as color conversion materials, quantum dots (QDs) are toxic and unstable, whereas commercially available inorganic phosphors are too big in size to combine with small mini-LED chips and also have strong size-dependence of quantum efficiency (QE) and reliability. In this work, we prepare fine-grained $Sr_2Si_5N_8:Eu^{2+}$-based red phosphors with high efficiency and stability by treating commercially available phosphors with ball milling, centrifuging, and acid washing. The particle size of phosphors can be easily controlled by milling speed, and the phosphors with a size varying from 3.5 to 0.7 μm are thus obtained. The samples remain the same QE as the original ones (~80%) even when their particle size is reduced to 3.2–3.5 μm, because they contain fewer surface suspension bond defects. More importantly, $SrBaSi_5N_8:Eu^{2+}$ phosphors show a size-independent thermal quenching behavior and a zero thermal degradation. We demonstrate that red-emitting mini-LEDs can be fabricated by combining the $SrBaSi_5N_8:Eu^{2+}$ red phosphor (3.5 μm in size) with blue mini-LED chips, which show a high external quantum efficiency (EQE) of above 31% and a super-high luminance of 34.3 Mnits. It indicates that fine and high efficiency phosphors can be obtained by the proposed method in this work, and they have great potentials for use in mini-LED displays.

Keywords: $Sr_2Si_5N_8:Eu^{2+}$-based phosphors; particle size; external quantum efficiency (EQE); thermal degradation; mini-LED

1 Introduction

With advances in the light extraction efficiency of minimized InGaN LED chips, mini-LED displays are attracting great attention in very recent years as they possess great advantages of high luminance, excellent contrast ratio (1,000,000:1), and superior high dynamic range (HDR) [1–3]. These promising properties make mini-LED displays affordable version of OLEDs but without screen burn-in issues [4–6], and thus are very attractive for use in a variety of applications, ranging

* Corresponding authors.
E-mail: S. Li, lishuxing@xmu.edu.cn;
G. Liu, gzliu1983@163.com;
R.-J. Xie, rjxie@xmu.edu.cn

from smart phones, large TVs, to automotive and industrial applications. Mini-LEDs can be used as the backlight source for a conventional liquid orystal display (LCD), or as self-emissive pixel emitters [3,7]. As for self-emissive displays, green and red mini-LED chips have unacceptable low efficiencies, so they are hardly used as individual emitters in full-color mini-LED displays at the current stage [3,8–10]. As for backlight units, blue mini-LED chips are usually used as a primary source to pump color conversion materials, such as quantum dots (QDs) and phosphors, which revives traditional LCDs and makes them much brighter and more vivid. Therefore, color conversion materials are a key component in this emerging display technology.

QDs have very promising optoelectronic properties, such as narrow emission bands, high quantum efficiency (QE), and tunable emission colors, making them more suitable for applications in wide-color-gamut displays. However, QDs are chemically unstable, toxic, and expensive [11]. Inorganic phosphors, which are thermally and chemically stable, are thus widely used as color conversion materials for LED backlights, including green-emitting β-sialon:Eu^{2+}, red-emitting $CaAlSiN_3$:Eu^{2+}, $Sr_2Si_5N_8$:Eu^{2+}, and K_2SiF_6:Mn^{4+} [12–16]. On the other hand, these phosphors usually have a particle size larger than 10 μm, which causes a low packing density of the color conversion layer and makes them unsuitable for use in mini-LED backlights for super-high resolution displays. To the best of our knowledge, no reports on fine phosphors for mini-LED backlights are now available. Therefore, it is necessary to develop phosphors with a much smaller particle size (e.g., < 5 μm) and high efficiency for realizing the mini-LED displays.

$Sr_2Si_5N_8$:Eu^{2+} is an excellent red phosphor for white LEDs owing to its high QE (> 80%) and high stability against chemical and thermal attacks [17,18]. It is commonly synthesized by using the solid-state reaction method at high temperatures (i.e., 1600–1800 ℃), and thus often has a particle size of about 20 μm [14]. To reduce the particle size, some low-temperature methods have been proposed for preparing the phosphor. Piao *et al*. [19] and Yang *et al*. [20] successfully obtained $Sr_2Si_5N_8$:Eu^{2+} phosphors at 1500–1550 ℃ by using the carbothermal reduction and nitridation (CRN) method, but the QE was significantly reduced to 28.4% due to the presence of residual carbon. Zeuner *et al*. [21,22] used the ammothermal method to synthesize nano-sized $Sr_2Si_5N_8$:Eu^{2+} phosphors with a particle size of 200 nm at 1150–1400 ℃, but it is difficult to obtain a pure phase. Size control of phosphor particles can also be achieved via carbon coating [23]. The amorphous carbon layer on the surface helps separate water and oxygen, and thus improves the hydrolysis resistance and thermal stability. However, this strategy reduces the photoluminescence intensity of the phosphor [24]. Alternatively, Kang *et al*. [25] prepared nano-sized $Sr_2Si_5N_8$:Eu^{2+} phosphors with an average particle size of 144 nm by pulverizing commercial phosphors via high-energy ball milling. Unfortunately, the QE of these nano phosphors was greatly decreased to 61% due to the destroyed surfaces.

In this work, we attempt to synthesize highly efficient and stable $Sr_2Si_5N_8$:Eu^{2+}-based phosphors ($Sr_2Si_5N_8$:Eu^{2+} and $SrBaSi_5N_8$:Eu^{2+}) with a particle size of several micrometers by high-energy ball milling and demonstrate their application in mini-LEDs. We demonstrate that the phosphor can maintain a QE as high as 80% and an excellent thermal stability even if the particle size is reduced to 3.2–3.5 μm. In addition, a prototype red-emitting mini-LED by using the fine $SrBaSi_5N_8$:Eu^{2+} phosphor as a color conversion material has a high external quantum efficiency (EQE) of above 31% and a super-high luminance of 34.3 Mnits.

2 Experimental

2.1 Pulverization of phosphor powders

The commercially available phosphors, $Sr_2Si_5N_8$:Eu^{2+} (ZYP630H) and $SrBaSi_5N_8$:Eu^{2+} (ZYP615G3C) (Beijing Nakamura Yuji Science and Technology Co., Ltd.) show irregular particles with an average particle size of ~10 μm. High-energy ball milling was used to reduce the particle size of phosphors by using a planetary miller (QM-QX, Nanjing Nanda Instrument Plant). The phosphor powders were mixed with ethyl alcohol and Si_3N_4 balls with a diameter of 2 mm, and the ratio of phosphor to alcohol to ball is 1:1:10 (in weight). The milling technique was 10 sets of 10 min with desired rotation speeds (300, 350, 400, and 500 r/min) and 10 min interrupt to prevent overheating. After ball milling, the phosphor powders with different target particle sizes were centrifugally separated by using a desktop high speed centrifuge at 1000 r/min for 1 min and the deionized water as a medium. Finally, the pulverized phosphor powders were acid washed by using 5 mol/L dilute hydrochloric acid. Then the phosphors were washed out with deionized water five times and dried at 80 ℃ overnight.

2. 2 Fabrication of red-emitting mini-LEDs

The red mini-LEDs were fabricated by combining the phosphor materials, i.e., fine-grained $SrBaSi_5N_8:Eu^{2+}$ or CdSe QDs (Xiamen Bohr Technology Co., Ltd.), with 450 nm InGaN mini-LED chips (100 μm × 200 μm, San'an Optoelectronics Co., Ltd.). Typically, 250 mg of phosphor materials were mixed with 500 mg of epoxy resin with vigorous stirring to form a uniform slurry. Next, the slurry was coated onto an InGaN mini-LED chip and cured under ambient conditions overnight.

2. 3 Characterizations

The X-ray diffraction (XRD) patterns were obtained by a powder X-ray diffractometer (D8 Advance, Bruker) under Cu Kα radiation (40 kV and 40 mA). The particle size of phosphor was measured by a laser particle size analyzer (LS-POP (9), Zhuhai OMEC Instrument Co., Ltd.). The microstructure was observed by a scanning emission microscopy (SEM; SU70, Hitachi) at an accelerated voltage of 5 kV. The high-resolution transmission electron microscope (HRTEM) characterization of the elemental mapping was obtained by an electron microscopy equipped with a field firing gun (Talos F200s, FEI). The QE was measured by using a self-built sphere-spectroradiometer system. The system consists of an excitation light source (50 mW single-mode blue laser diode, the emission peak λ_{em} = 450 nm) and an integrated sphere (15 cm in diameter) connected to a charge-coupled device (CCD) spectrometer (USB2000+, Ocean Optics). The photoluminescence excitation (PLE) and emission spectra were recorded on a steady-state fluorescence spectrometer (FLS980, Edinburgh Instruments) equipped with a 450 W xenon lamp. The thermal degradation and thermal quenching were measured by using a home-made measurement system consisting of a 450 nm LED light source, a cooling/heating stage (THMS600E, Linkam Scientific Instruments), and a CCD spectrometer (USB2000+, Ocean Optics). The PL intensity imaging of single particles was recorded by a Q2 time-resolved confocal imaging system (FILM, ISS Inc). It uses a Nikon 60X/1.2NA water objective in conjunction with the Nikon TIU microscope. A 405-nm pulsed laser diode was used as the excitation source. Both the laser and scanner were synchronized with the ISS Fast FLIM data acquisition unit to record the time-resolved data for each pixel of the image. The electron spin resonance (ESR) curves were recorded at room temperature (RT) by an ESR spectrometer (A300, Bruker). The obtained mini-LEDs were evaluated by using a commercialized system (XPQY-EQE, Xi Pu Guang Dian Co., Ltd.).

3 Results and discussion

Commercially available red phosphors of $Sr_2Si_5N_8:Eu^{2+}$ and $SrBaSi_5N_8:Eu^{2+}$ (labelled as S and S/B hereinafter), having an emission maximum of 625 and 618 nm respectively, were chosen for investigations in this work. Their phase purity and element compositions were confirmed by the XRD patterns and energy-dispersive X-ray spectroscopy (EDS) mapping images, respectively (Fig. S1 in the Electronic Supplementary Material (ESM)). Phosphor powders with different particle sizes (i.e., D_{50}) were obtained by ball-milling the commercial raw powders with varying milling speeds, followed by the centrifugation and acid washing. The milled powders undergo no phase transformation during the pulverization (Figs. S2(a) and S2(b) in the ESM). The D_{50} value decreases from 11.2/12.3 μm to 3.2/3.5 μm, further to ~0.7 μm by increasing the milling speed. The treated samples were then labelled as S-1–4 and S/B-1–4 with decreasing the particle size, and the original powders were labelled as S-0 and S/B-0, respectively. As seen in Figs. 1(a) and 1(b), all the treated samples show a narrow and unimodal particle size distribution, indicating a uniform morphology. It is also confirmed by the SEM images (Fig. 1(c) and Fig. S2(c) in the ESM) that the S/B-1–4 samples demonstrate fine and uniform particles separated from each other, but the original one is obviously aggregated and has a rodlike shape.

As given in Fig. 2, the QE and absorption of the as-treated samples generally declined from 75%/80% to 40%/59% with the particle size decreasing from 11.2/12.3 to 0.7 μm due to the broken surface and the enhanced scattering. It is worth noting that the samples with an average particle size of 3.2 or 3.5 μm have a very close QE to the original phosphors, which is 75% and 80% for S-1 and S/B-1, respectively. As the particle size decreases, the shape of the calibrated emission spectra keeps almost unchanged, whereas that of the calibrated excitation spectra shows a decrease in intensity at wavelengths longer than 300 nm (Fig. S3 in the ESM). It is attributed to the weakened coupling probability between phonons and excitation photons for small-sized phosphor particles [26]. The thermal quenching and thermal degradation of Groups S and

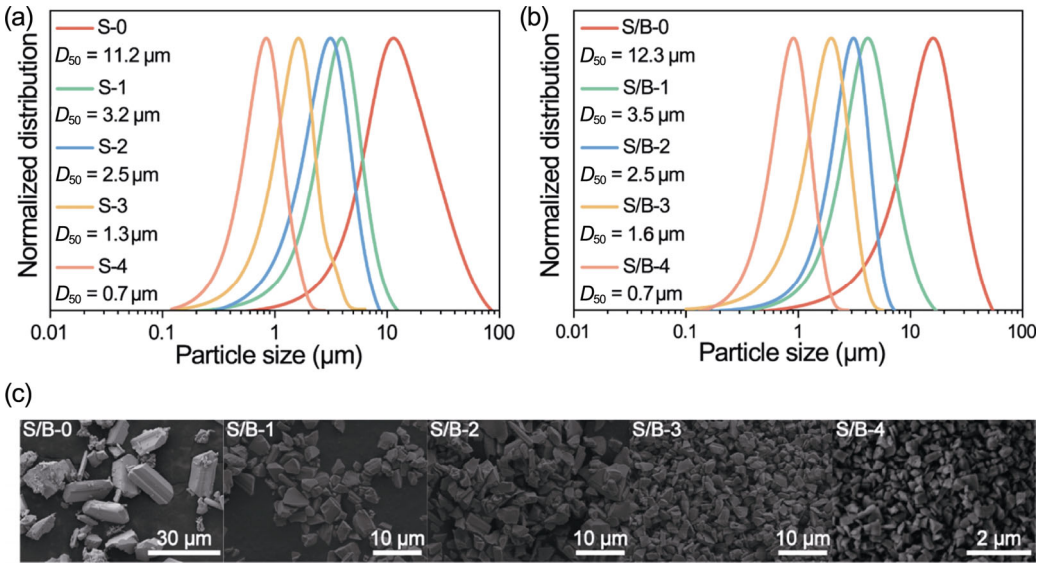

Fig. 1 Particle size distribution curves of (a) Groups S-0–4 and (b) Groups S/B-0–4; (c) SEM images of Groups S/B-0–4. The samples were labelled depending on the particle size.

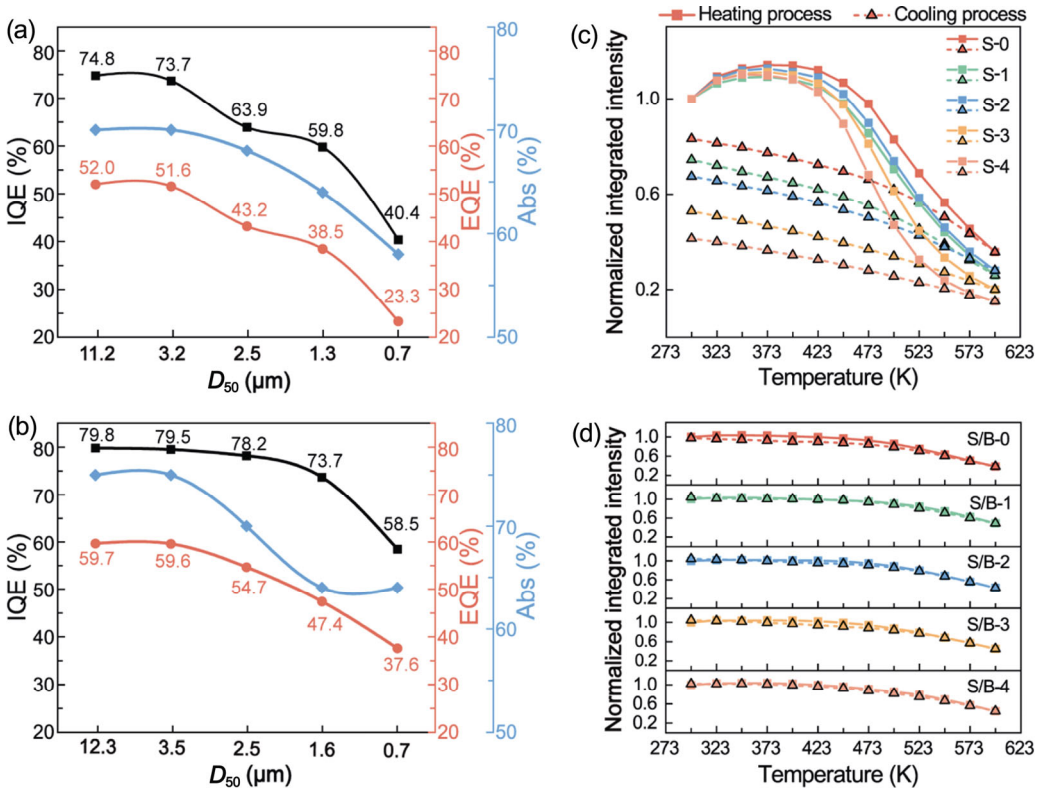

Fig. 2 (a, b) Internal quantum efficiency (IQE, black solid line), EQE (red solid line), and absorption efficiency (Abs, blue solid line) as a function of D_{50} in Group S and S/B, respectively; (c, d) temperature-dependent emission intensity (integrated) of samples in Groups S and S/B, respectively.

S/B were evaluated by heating them from room temperature (RT) to 598 K and then cooling them back to RT. As shown in Figs. 2(c) and 2(d), one can find that the samples of Group S have poor thermal stability, but those of Group S/B exhibit excellent thermal stability. With decreasing the particle size, both thermal quenching and thermal degradation turn worse for Group S. When the temperature increases, the emission intensity decreases, and the emission spectra broaden simultaneously (Fig. S4 in the ESM). The

spectral broadening of Group S is more obvious than that of Group S/B. As a result, the integrated temperature-dependent emission intensity of Group S increases, while that of Group S/B decreases during heating from 298 to 373 K. When the samples are heated to 473 K, the loss in emission intensity is only 2% for S-0 (D_{50} = 11.2 μm), but it increases up to 32% for S-4 (D_{50} = 0.7 μm). The luminescence quenching is more significant as the temperature further increases. During the cooling cycle (598 K → RT), serious thermal degradation occurs, i.e., the emission intensity is lost by 17% for S-0 and by 59% for S-4. On the other hand, all the samples of Group S/B only lose less than 10% in emission intensity at 473 K, and show zero thermal degradation after the heating–cooling cycle, indicating that the thermal stability of $Sr_2Si_5N_8$:Eu^{2+} can be enhanced by the Ba substitution and is particle size independent. Thermal degradation of Group S can be attributed to the oxidation of Eu^{2+} to Eu^{3+} [27,28]. As the particle size is reduced, the surface oxidation occurs more easily with an increasing amount of Eu^{2+} exposed on the surface, causing more serious thermal degradation [29]. As for Group S/B, the Sr/Eu–N bond has stronger covalence than the Ba–N bond [28], and thus Ba is more susceptible to bond with O than Eu, which therefore protects Eu^{2+} from oxidation to some extent, and leads to zero thermal degradation even when the phosphor particles become smaller. These results validate that the thermally robust $SrBaSi_5N_8$:Eu^{2+} phosphor is more suitable for use as color conversion material in mini-LEDs.

To further understand the luminescence of fine-grained phosphors in Group S/B, the mappings of photoluminescence intensity and decay time were recorded by using a fluorescence lifetime imaging microscope (FLIM) under 405 nm excitation. As shown in Figs. 3(a) and 3(b), each phosphor particle shows uniform luminescence intensity and decay time mappings. The decay time distribution of all samples shows a unimodal shape and becomes narrower with decreasing the particle size. The average decay time keeps almost constant for S/B-0 (1.22 μs), S/B-1 (1.22 μs), and S/B-2 (1.20 μs), but decreases to 0.95/0.94 μs for S/B-3 and S/B-4, respectively. The decrease in decay time is consistent with that of the IQE value (Fig. 2(b)). During the pulverization process, the surface of phosphor particles is destroyed by strong collision, and some surface defects will be inevitably formed, thus enhancing the non-radiative energy transfer and reducing the QE as well as decay time. This phenomenon has also been observed in other phosphors, such as $CaYAl_3O_7$:Eu^{3+} and $LaPO_4$:Ce^{3+},Tb^{3+} [30–32]. Although the phosphor particles are broken, they still have good crystallinity, and no amorphous layer is seen on the surface, as revealed by the transmission electron microscopy (TEM) images (Fig. S5 in the ESM).

To clarify the origin of the size-dependent QE, the ESR spectra of Group S/B were measured. As plotted in Fig. 4, the *g*-values of 4.399 and 4.197 can be attributed to the Eu^{2+} dopant, of which the signal intensity does not change during pulverization. The signal at a *g*-value of 2.003 is generally attributed to a neutral *K*-center, which is originated from silicon dangling bonds with different neighboring atoms [33–35]. As seen in Fig. 4(b), it is gradually intensified with decreasing particle size and is much stronger for S/B-4. It indicates that more surface suspension bond defects are generated, which increases the probability of non-radiative energy

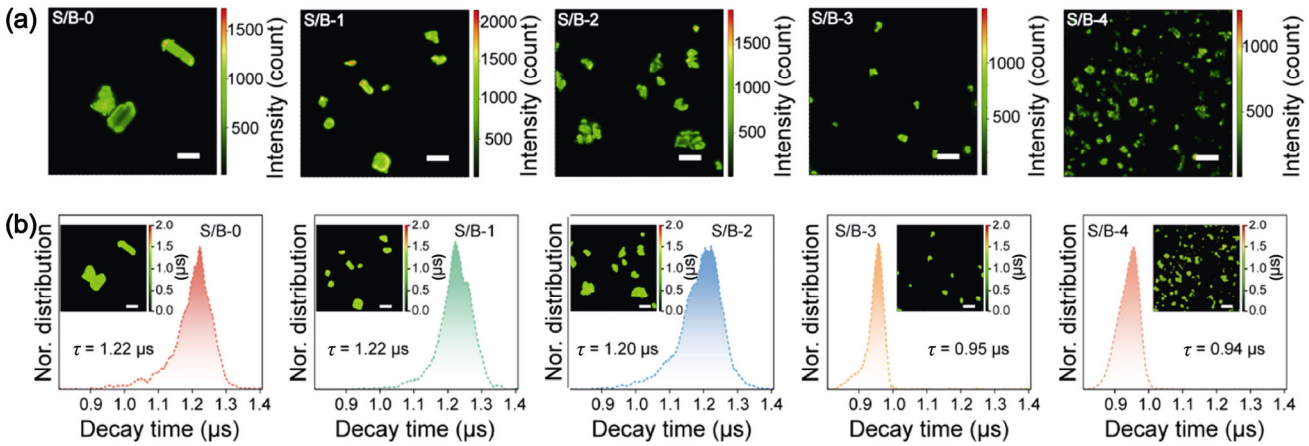

Fig. 3 (a) Fluorescence microscopy images under 405 nm laser excitation (scale bars are 10 μm); (b) decay time distribution curves calculated by an FLIM, and the insets are the decay time mapping images (scale bars are 10 μm).

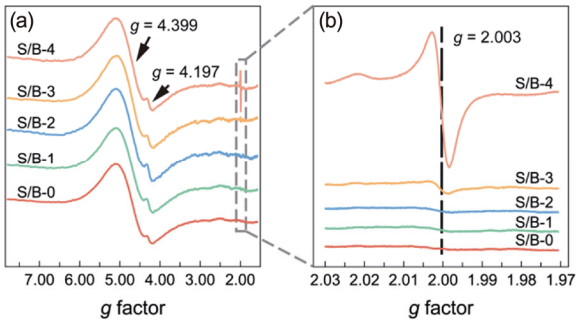

Fig. 4 (a) ESR spectra of Group S/B recorded at RT; (b) locally zoomed ESR.

transfer, and therefore reduces the QE of the pulverized phosphors.

The samples in Group S/B were applied to fabricate red-emitting mini-LEDs by combining them with blue mini-LED chips (λ_{em} = 450 nm, EQE > 46%). The blue mini-LED chip has a geometrical size of 100 μm × 200 μm. For reference, commercially available red-emitting CdSe QDs were also coupled with blue mini-LED chips (Figs. 5(a) and 5(b)). As shown in Table 1, the red-emitting mini-LEDs by using S/B-1 and S/B-2 have the highest saturation current of 60 mA and the luminance maxima of 34.3 and 27.8 Mnits, respectively. Although S/B-0 has a higher QE than S/B-1 and S/B-2, the lower packing density of the coarse particles finally yields a lower luminance. For CdSe QDs, they have a high QE but a weak absorption in the blue light region. As a result, the peak luminance of the red-emitting mini-LEDs by using CdSe QDs is only 25% of that by using S/B-1. Moreover, the red-emitting mini-LEDs by using S/B-1 also show an ultrahigh EQE of over 31% at a small current (< 1 mA), whereas the AlGaInP semiconductor red-emitting mini-LEDs usually have an EQE of < 20% [3]. The red-emitting mini-LED by using S/B-1 exhibits a high luminance of 2.6 Mnits and an EQE value of 31% (Fig. S6 in the ESM). In addition, the emission spectra of the mini-LEDs do not change in shape and peak position when the current is increased from 10 to 70 mA (Fig. 5(c)). A lightened mini-LED is demonstrated, showing bright red light when driven at 30 mA (Fig. 5(d)). These results imply that the fine-grained $SrBaSi_5N_8:Eu^{2+}$ phosphor is an excellent red-emitting color conversion material for next-generation mini-LED displays.

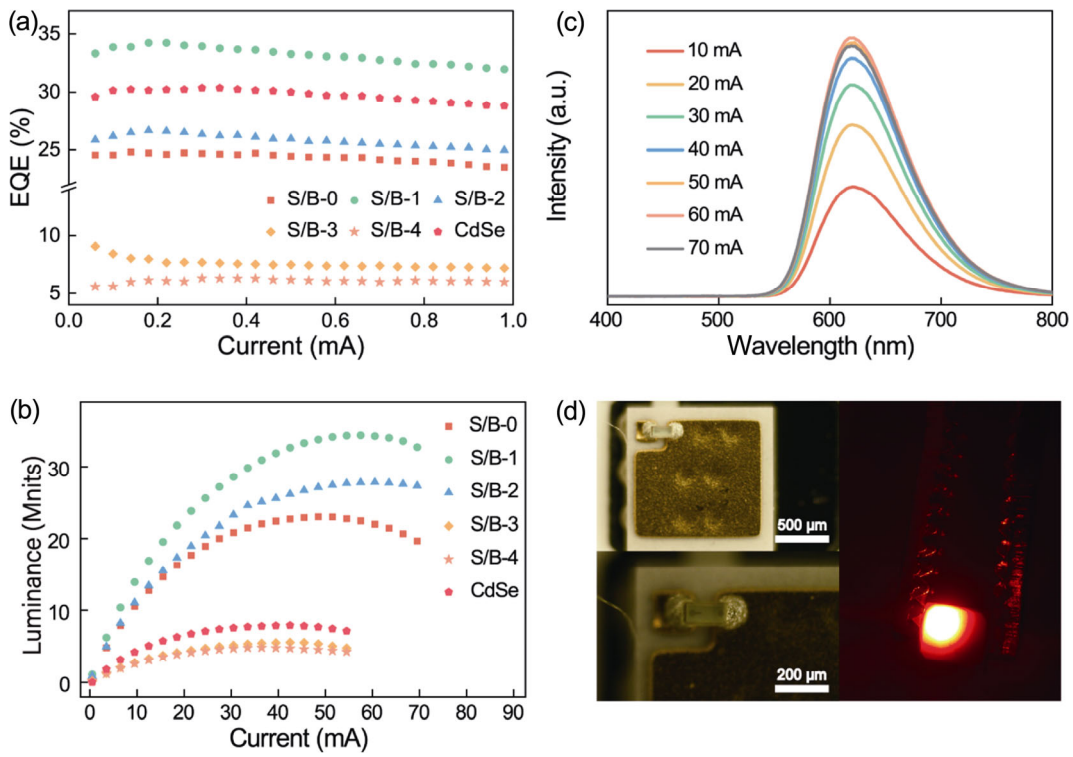

Fig. 5 (a) Current-dependent EQEs of the as-fabricated red-emitting mini-LEDs by using Group S/B or commercial CdSe QDs and (b) luminance–current curves; (c) emission spectra of the red-emitting mini-LEDs fabricated with S/B-1 and (d) corresponding photograph pumped at 30 mA.

Table 1 Saturation currents and peak luminance of the as-fabricated red-emitting mini-LEDs by using S/B-0–4 and CdSe QDs

Sample	Saturation current (mA)	Peak luminance (Mnits)
S/B-0	50	23.0
S/B-1	60	34.3
S/B-2	60	27.8
S/B-3	45	5.5
S/B-4	35	4.8
CdSe	40	7.9

4 Conclusions

In summary, fine-grained $Sr_2Si_5N_8:Eu^{2+}$-based phosphors with a particle size of 0.7–3.5 μm were successfully prepared via simple milling, centrifuging, and acid washing. Both $Sr_2Si_5N_8:Eu^{2+}$ and $SrBaSi_5N_8:Eu^{2+}$ phosphors remain an unchanged IQE of ~80% even when their particle size is reduced to 3.2–3.5 μm, and $SrBaSi_5N_8:Eu^{2+}$ shows a size-independent thermal quenching behavior and a zero thermal degradation. The QE starts to decline with further reduced phosphor particle size due to the creation of surface dangling bonds that lead to the non-radiative energy relaxation. A red-emitting mini-LED is demonstrated by pumping the $SrBaSi_5N_8:Eu^{2+}$ phosphor (with a size of 3.5 μm) with a blue mini-LED chip (λ_{em} = 450 nm, EQE > 46%), which shows a high luminance of 34.3 Mnits under 60 mA and an ultrahigh EQE of over 31% at low pumping currents (< 1 mA). This phosphor-converted red-emitting mini-LED exhibits superior photoelectric properties over the AlGaInP semiconductor mini-LED chip. This work indicates that the fine-grained $SrBaSi_5N_8:Eu^{2+}$ phosphor can be used as a promising red-emitting color conversion material for next-generation mini-LED displays.

Acknowledgements

This work is supported by the National Natural Science Foundation of China (Nos. 51832005 and 52172157), the Fundamental Research Funds for the Central Universities (No. 20720200075), and Fujian Provincial Science and Technology Project (Nos. 2020I0002 and 2021J01042).

Declaration of competing interest

The authors have no competing interests to declare that are relevant to the content of this article.

Electronic Supplementary Material

Supplementary material is available in the online version of this article at https://doi.org/10.1007/s40145-022-0617-z.

References

[1] Tan GJ, Huang YG, Li MC, *et al*. High dynamic range liquid crystal displays with a mini-LED backlight. *Opt Express* 2018, **26**: 16572–16584.

[2] Huang YG, Tan GJ, Gou FW, *et al*. Prospects and challenges of mini-LED and micro-LED displays. *J Soc Inf Display* 2019, **27**: 387–401.

[3] Huang YG, Hsiang EL, Deng MY, *et al*. Mini-LED, Micro-LED and OLED displays: Present status and future perspectives. *Light Sci Appl* 2020, **9**: 105.

[4] Zhou X, He J, Liao LS, *et al*. Real-time observation of temperature rise and thermal breakdown processes in organic LEDs using an IR imaging and analysis system. *Adv Mater* 2000, **12**: 265–269.

[5] So F, Kondakov D. Degradation mechanisms in small-molecule and polymer organic light-emitting diodes. *Adv Mater* 2010, **22**: 3762–3777.

[6] Kirch A, Fischer A, Liero M, *et al*. Electrothermal tristability causes sudden burn-in phenomena in organic LEDs. *Adv Funct Materials* 2021, **31**: 2106716.

[7] Hsiang EL, Yang Q, He ZQ, *et al*. Halo effect in high-dynamic-range mini-LED backlit LCDs. *Opt Express* 2020, **28**: 36822–36837.

[8] Even A, Laval G, Ledoux O, *et al*. Enhanced in incorporation in full InGaN heterostructure grown on relaxed InGaN pseudo-substrate. *Appl Phys Lett* 2017, **110**: 262103.

[9] Auf der Maur M, Pecchia A, Penazzi G, *et al*. Efficiency drop in green InGaN/GaN light emitting diodes: The role of random alloy fluctuations. *Phys Rev Lett* 2016, **116**: 027401.

[10] Guo WJ, Chen N, Lu H, *et al*. The impact of luminous properties of red, green, and blue mini-LEDs on the color gamut. *IEEE Trans Electron Devices* 2019, **66**: 2263–2268.

[11] Moon H, Lee C, Lee W, *et al*. Stability of quantum dots, quantum dot films, and quantum dot light-emitting diodes for display applications. *Adv Mater* 2019, **31**: e1804294.

[12] Li SX, Wang L, Tang DM, *et al*. Achieving high quantum efficiency narrow-band β-sialon:Eu^{2+} phosphors for high-brightness LCD backlights by reducing the Eu^{3+} luminescence killer. *Chem Mater* 2018, **30**: 494–505.

[13] Zhou TY, Hou C, Zhang L, *et al*. Efficient spectral regulation in $Ce:Lu_3(Al,Cr)_5O_{12}$ and $Ce:Lu_3(Al,Cr)_5O_{12}$/$Ce:Y_3Al_5O_{12}$ transparent ceramics with high color rendering index for high-power white LEDs/LDs. *J Adv Ceram* 2021, **10**: 1107–1118.

[14] Xie RJ, Hirosaki N, Takeda T. Wide color gamut backlight for liquid crystal displays using three-band phosphor-

converted white light-emitting diodes. *Appl Phys Express* 2009, **2**: 022401.

[15] Wang L, Xie RJ, Suehiro T, *et al*. Down-conversion nitride materials for solid state lighting: Recent advances and perspectives. *Chem Rev* 2018, **118**: 1951–2009.

[16] Zhou YY, Song EH, Deng TT, *et al*. Surface passivation toward highly stable Mn^{4+}-activated red-emitting fluoride phosphors and enhanced photostability for white LEDs. *Adv Mater Interfaces* 2019, **6**: 1802006.

[17] Brinkley SE, Pfaff N, Denault KA, *et al*. Robust thermal performance of $Sr_2Si_5N_8:Eu^{2+}$: An efficient red emitting phosphor for light emitting diode based white lighting. *Appl Phys Lett* 2011, **99**: 241106.

[18] Hua H, Feng SW, Ouyang ZY, *et al*. YAGG:Ce transparent ceramics with high luminous efficiency for solid-state lighting application. *J Adv Ceram* 2019, **8**: 389–398.

[19] Piao XQ, Horikawa T, Hanzawa H, *et al*. Characterization and luminescence properties of $Sr_2Si_5N_8:Eu^{2+}$ phosphor for white light-emitting-diode illumination. *Appl Phys Lett* 2006, **88**: 161908.

[20] Yang YF, Chen JJ, Li GH, *et al*. Synthesis of nitride phosphor using entire oxides raw materials and their photoluminescence properties. *J Am Ceram Soc* 2017, **100**: 1022–1029.

[21] Zeuner M, Hintze F, Schnick W. Low temperature precursor route for highly efficient spherically shaped LED-phosphors $M_2Si_5N_8:Eu^{2+}$ (M = Eu, Sr, Ba). *Chem Mater* 2009, **21**: 336–342.

[22] Zeuner M, Schmidt PJ, Schnick W. One-pot synthesis of single-source precursors for nanocrystalline LED phosphors $M_2Si_5N_8:Eu^{2+}$ (M = Sr, Ba). *Chem Mater* 2009, **21**: 2467–2473.

[23] Chen HR, Ju LC, Zhang L, *et al*. Exploring a particle-size-reduction strategy of YAG:Ce phosphor via a chemical breakdown method. *J Rare Earths* 2021, **39**: 938–945.

[24] Liu YX, Wang H, Chen DY, *et al*. Achieving thermally stable and anti-hydrolytic $Sr_2Si_5N_8:Eu^{2+}$ phosphor via a nanoscale carbon deposition strategy. *Ceram Int* 2021, **47**: 3244–3251.

[25] Kang T, Lee S, Kim T, *et al*. Efficient luminescence of $Sr_2Si_5N_8:Eu^{2+}$ nanophosphor and its film applications to LED and Solar cell as a downconverter. *Sci Rep* 2020, **10**: 1475.

[26] Zhang JZ. Ultrafast studies of electron dynamics in semiconductor and metal colloidal nanoparticles: Effects of size and surface. *Acc Chem Res* 1997, **30**: 423–429.

[27] Liu LH, Wang L, Li YQ, *et al*. Structural evolutions and significantly reduced thermal degradation of red-emitting $Sr_2Si_5N_8:Eu^{2+}$ via carbon doping. *J Mater Chem C* 2017, **5**: 8927–8935.

[28] Yeh CW, Chen WT, Liu RS, *et al*. Origin of thermal degradation of $Sr_{2-x}Si_5N_8:Eu_x$ phosphors in air for light-emitting diodes. *J Am Chem Soc* 2012, **134**: 14108–14117.

[29] Bizarri G, Moine B. On $BaMgAl_{10}O_{17}:Eu^{2+}$ phosphor degradation mechanism: Thermal treatment effects. *J Lumin* 2005, **113**: 199–213.

[30] Dwivedi J, Kumar P, Kumar A, *et al*. A commercial approach for the fabrication of bulk and nano phosphors converted into highly efficient white LEDs. *RSC Adv* 2014, **4**: 54936–54947.

[31] Yim CJ, Unithrattil S, Chung WJ, *et al*. Comparative study of optical and structural properties of electrospun 1-dimensional $CaYAl_3O_7:Eu^{3+}$ nanofibers and bulk phosphor. *Mater Charact* 2014, **95**: 27–35.

[32] Zhu HL, Zhu EZ, Yang H, *et al*. High-brightness $LaPO_4:Ce^{3+},Tb^{3+}$ nanophosphors: Reductive hydrothermal synthesis and photoluminescent properties. *J Am Ceram Soc* 2008, **91**: 1682–1685.

[33] Kolodiazhnyi T, Golberg D. Paramagnetic defects in boron nitride nanostructures. *Chem Phys Lett* 2005, **413**: 47–51.

[34] Umeda T, Mochizuki Y, Miyoshi Y, *et al*. Charge-trapping defects in Cat-CVD silicon nitride films. *Thin Solid Films* 2001, **395**: 266–269.

[35] Rebib F, Tomasella E, Aida S, *et al*. Influence of the structure of a-SiO_xN_y thin films on their electrical properties. *Plasma Process Polym* 2007, **4**: S59–S63.